Contents lists available at ScienceDirect

Applied Thermal Engineering

journal homepage: www.elsevier.com/locate/apthermeng

Research Paper

Manufacturing and experimental analysis of a dew-point indirect evaporative cooler using fused deposition modelling 3D printing and polymeric materials

Jesús Castillo-González [a], Francisco Comino [b,*], Francisco J. Navas-Martos [a], Manuel Ruiz de Adana [c]

[a] Centro Tecnológico del Plástico Andaltec, Calle Vilches 34, Ampliación Polígono Cañada de la Fuente, 23600 Martos Jaén, Spain
[b] Departamento de Mecánica, Escuela Politécnica Superior, Universidad de Córdoba, Campus de Rabanales, Antigua Carretera Nacional IV, km 396, 14071 Córdoba, Spain
[c] Departamento de Química-Física y Termodinámica Aplicada, Escuela Politécnica Superior, Universidad de Córdoba, Campus de Rabanales, Antigua Carretera Nacional IV, km 396, 14071 Córdoba, Spain

ARTICLE INFO

ABSTRACT

Evaporative cooling (EC) is an interesting alternative for reducing energy consumption and CO_2 emission associated with the cooling of building. In the present work, a prototype of an innovative dew-point indirect evaporative cooler (DIEC) was manufactured by additive manufacturing technology. This prototype was made up of two types of materials: (a) one porous, with high water absorption capacity, polyvinyl alcohol (PVA) with felt, and therefore, high capacity of generate EC; and (b) another with high hydrophobic properties, polylactic acid (PLA) with bronze. The materials were characterised in terms of thermal, water absorption properties and morphological properties. Prior to manufacturing, a design of experiments was conducted in order to find the optimal manufacturing parameters. The prototype was produced through an innovative process, based on the simultaneous use of two extruders, and the manufacture of a porous layer of felt by dissolving the PVA matrix where the felt was initially embedded. Finally, the energy performance of the prototype was experimentally analysed, reaching values of dew-point effectiveness up to 0.9 and energy efficiency ratio up to 22.74 at 45 °C outside dry bulb temperature. These results show that additive manufacturing is promising for developing competitive compact and highly energy efficient DIEC systems.

1. Introduction

The rise in temperature of the earth's surface has led to a sharp increase in the demand for cooling in buildings [1]. Currently, 20% and 40% of the world and European energy consumption and its related CO_2 emission are generated in the building sector [2]. Most Heat Ventilation Air Conditioning system (HVAC) are based on conventional vapour-compression cycles, which depend mainly on electrical energy [3]. Therefore, evaporative cooling (EC) systems are nowadays presented as an interesting low-energy consumption alternative for building cooling [4]. Traditional EC systems are able to reduce the supply air temperature only up to the inlet wet-bulb temperature, however dew point indirect evaporative cooler (DIEC) are capable or reducing supply air temperature up to the inlet dew point temperature [5].

When it comes to HVAC manufacturing, Additive Manufacturing (AM) is a promising technique. Previous work carried out by other researchers in the framework of HVAC manufacturing using AM technologies is summarised in Table 1. These research demonstrate the suitability of AM for some applications in HVAC industry: in the manufacturing of Heat Exchanger (HX) [6–11] and HVAC insulation [12]. In general, AM is presented as an alternative tool with great potential for the manufacture of some HVAC components [13].

Furthermore, some authors studied HXs developed with AM techniques and polymeric materials for other application different to HVAC, following are summarised some of them. Authors presented a review on additively manufactured HXs and presented polymeric materials like a suitable option [14]. The thermal performance of a HX made with a graphene-charged PLA filament was analysed and compared to another made with conventional ABS filament, achieving a slightly better energy

---

* Corresponding author.
E-mail address: francisco.comino@uco.es (F. Comino).

Nomenclature

c_p	specific heat [kJ/kg K]
EER	energy efficiency ratio [-]
F	flow [%]
h	enthalpy [kJ/kg]
N	test number
Q	thermal energy [kJ]
$\dot{Q}$	thermal power [kW]
R	ratio of volumetric air flow rate
Ra	average roughness, average difference between peaks and valleys in a reference line [μm]
Rq	mean squared of the roughness profile deviation in a reference line [μm]
Rt	maximum distance between peak and valley in a reference line [μm]
Rz	average of the maximum peak-valley distances in a reference line [μm]
Sa	arithmetic mean height of the whole surface [μm]
Sp	maximum peak height in the whole surface [μm]
Sq	mean squared of the height in the whole surface [μm]
Sv	maximum valley depth in the whole surface [μm]
Sz	maximum distance between peak-valley in the whole surface [μm]
t	time [min]
T	temperature [°C]
V	extrusion speed [mm/s]
$\dot{V}$	volumetric air flow rate
W	water absorbed with respect to the weight of the dry samples [%]
$\dot{W}$	electric power [kW]
Z	layer height [mm]

Greek letters

Δ	increment, decrement
ε	effectiveness [-]
ρ	density [kg/m^3]
α	diffusivity [m^2/s]
σ	conductivity [W/m·K]
η	efficiency [-]

Subscripts

d	dew point
e	exhaust
i	inlet
SA	supply air

Acronyms

AHU	air handing unit
AM	additive manufacturing
CAD	computer aided design
DEC	direct evaporative cooling
DIEC	dew-point indirect evaporative cooling
DOE	design of experiment
DSC	differential scanning calorimetry
EC	evaporative cooling
FC	flow conditioner
FFF	fused filament fabrication
HDT	heat deflection temperature [°C]
HVAC	heat ventilation air conditioning
HX	heat exchanger
IEC	indirect evaporative cooling
JQH	layer joining and surface quality in hydrophobic material
JQP	layer joining and surface quality in porous material
NTU	number of transfer units
PCM	phase change material
PLA	polylactic acid
PVA	polyvinyl alcohol
PT	pilot tube
SEM	scanning electron spectroscopy
SH	degree of string formation in the hydrophobic material
SP	string formation in the porous material
WSP	water absorbed at saturation point with respect to the weight of the dry samples [%]
W10M	water absorbed in the first 10 min with respect to the maximum water absorption [%]

exchange with grapheme-charged PLA [15]. A new air-cooled HX consisting of bifurcated bare tubes was numerically studied and fabricated by AM using polymeric materials, the prototype was found to have a 15% higher heat transfer coefficient than a baseline bare tube HX [16]. The manufacture of a HX with a gyroid structure by means of polymeric AM was studied achieving overall heat transfer coefficient up to 79.6 W/m^{2}K^1 [17]. Printed ABS HXs with staggered pin fins demonstrated that printability of small features is advantageous for improving performance of HX [18]. Additionally, other authors investigated the fabrication of high-temperature HXs using AM [14,19–21].

Most of the research on AM and HVAC presented in Table 1 manufactured and studied HX, nonetheless, none of these works studied the manufacturing of HX for DIEC systems by means of AM. DIEC systems are based on HXs with complex designs aimed at improving their exchange efficiency. AM allows manufacturing components with innovative geometries which are not possible or are too expensive to produce with conventional manufacturing technologies [22], therefore AM could be an interesting technique to develop HXs of DIEC system. In general, AM techniques can reduce material waste up to 80% and energy consumption up to 70% [23]. Moreover, AM allows to control the roughness and, therefore, to adjust the convective heat transfer and pressure drop [19,24]. A high roughness is advantageous for enhancing heat transfer but not to decrease pressure drop [25]. However, AM also faces some challenges such as: achieving higher production rates, eliminating unwanted porosity and defects, achieving properties similar to those obtained by injection moulding technology, and being able to generate complex geometries without wasting material on support structures [23].

The low thermal conductivity of the most commonly used polymer materials in AM, 0.1–0.5 W/m K [17,26], could be a drawback. Nevertheless, there is research to improve the thermal conductivity of polymer material parts, for example by adding highly conductive additives [27]. Some authors integrated carbon nanotubes into the polymer matrix, reaching thermal conductivities between 5 W/m K and 41 W/m K, depending on the percentage, orientation and properties of the filler [27]. Other authors studied other types of graphene-based fillers [28,29]. If highly conductive fibres are selected as an additive, it must be taken into account that the thermal conductivity increases significantly much more in the direction of fibre orientation. This material is not advantageous for DIEC system manufacturing due to this type of system requires more thermal conductivity in the direction perpendicular to which the fibre is oriented [30]. Other authors also decreased the thickness of the HX walls in order to reduce their thermal resistance, hence improving their heat transfer. AM allows walls of up to 0.4–0.5 mm to be manufactured, supporting this wall on other thicker walls [31].

Conventionally, DIEC systems are manufactured from different sheets separated by corrugated sheets or bars positioned parallel to the

Table 1

Recent research focused specifically on the application of AM in HVAC.

Reference	HVAC topic	AM topic	Main results	Year of publication
[6]	System involves a HX manufactured using polymer materials	Creation of microchannels within the HX	Resulting HX transfers 55% more thermal energy than a conventional system	2022
[7]	System involves HX	HX Manufactured from a polymer filled with thermally conductive material and using a continuous path for each layer deposited to prevent water leakage	Better thermal performance than using conventional technology	2023
[12]	Development of PCM materials for a more efficient storage of thermal energy in buildings	Integration of PCM materials into complex geometries for advance thermal management by using AM	Non-commercial PCM polymer composites materials filaments with outstanding properties	2022
[8]	System involves HX	State-of-the-art in HX additive manufacturing	AM improve thermal performance and reduce cost in HX manufacturing, but reduce quality comparing with conventional techniques	2021
[10]	System involves HX	Manufacture of polymer HXs for adsorption cooling manufactured by AM	Competitive systems in terms of thermodynamic performance with respect to another made of metallic material	2021
[9]	System involves HX	3D-printed polymer plate HX	HX made of thermoplastic using AM shows slightly better results than other made of aluminium	2021
[11]	System involves HX	HX manufactured by AM and using metal fibre as filler of the polymer matrix	220% and 125% improvement in heat flow rate over mass and over volume respectively	2020

airflow direction. The sheets are made by coating a hydrophobic material (dry channel) over a porous material (wet channel). The generated hydrophobic surface enables the inlet air to go through the dry duct without modifying its humidity. While the porous material allows to retain water and humidify and cool the air [32]. The most influential properties for porous material are fast and high water absorption capacity, low cost, and poor thermal contact resistance. In recent years, porous materials such as coconut, cellulose, palash, jute tossa, palm stem, luffa gourd, aspen wood excelsior, kraft and felt paper have been used in EC systems [33,34]. Usually, all these fibres have a good

permeability leading to high water evaporation [35]. Regarding hydrophobic material properties, DIEC systems require materials with a large surface area for efficient heat exchange. However, as the size of the equipment rise, the weight and cost of the equipment increase. Metals have traditionally been used as a hydrophobic material for DIEC systems, nevertheless other options are currently being studied. Some of these alternatives are different types of plastic films due to its low weight: high density polyethylene (HDPE) [36,37], polyurethane (PU) [37,38], polycarbonate (PC) [37], polypropylene (PP) [39].

Knowing the conventional way of DIEC manufacturing and AM advantages and disadvantages, although no bibliography was found, AM could be an innovative candidate for the manufacture of DIEC systems, especially, by using Fused Filament Fabrication (FFF), as this technology enables efficient manufacturing of parts from multiple materials. Thermal conductivity of these materials could be a disadvantage, nevertheless, this parameter is not as crucial as water absorption capacity of the porous materials in the DIEC systems [40]. Several researchers have worked in the field of using the FFF filaments to produce parts with high porosity. For example, manufacturing scaffolds for the medical application of bone regeneration [41–43], water filtration systems [44], sound absorbers [45] and membranes [46].

Considering all of the above, the main objective of this work was to address an important gap that exists today in the scientific literature in the field of DIEC systems: design, manufacture and evaluate a DIEC prototype developed from two different materials, one porous and the other hydrophobic, through FFF technology. This innovation has the following advantages: i) it avoids the need for assembly, since the entire IEC system is manufacture in a single piece; ii) it enables to manufacture complex geometries, generating a more efficient energy exchange; iii) it allows to use recycled polymer material as well as to easy recycling of the materials of the different components of the IEC system at the end of its useful life. In order to reach this goal, the thermal conductivity, wettability and roughness of various materials were studied. A detailed mathematical model of DIEC system developed previously [47] was used to obtain the final design of the prototype. Finally, the energy performance of the manufactured prototype was analysed.

2. Material and methods

The specific methodology conducted in this work was summarised in Fig. 1. In the following sections, all the tasks presented in the flowchart are described and explained in more detail.

2.1. Brief description of dew-point indirect evaporative cooling system

In the present work, a dew-point indirect evaporative cooler was manufactured and analysed experimentally. The manufactured system was based on a cross-flow HX. A schematic of various dry channels and wet channels is shown in Fig. 2. These DIEC systems handle 100% outside air (inlet air). Outside air enters through the dry channels, reducing the air temperature, due to heat exchange between the dry and wet channels. At the end of the dry channels there are perforations, which allow a percentage of the inlet air flow to be returned. The return air is in direct contact with a film of water, so there is an exchange of heat and mass between air and water, until it is expelled to the outside (exhaust air). The percentage of remaining inlet air is the supply air. The percentages of supplied air and returned air can be regulated with a damper downstream of the system, generating an overpressure. The water from the wet channels enters from the top of the system, wetting the hydrophilic walls, in order to obtain a thin layer of water. The excess water is expelled from the bottom of the system and returned to the top.

2.2. Materials and manufacturing method used for the manufacture of the channels

Two materials were selected for the fabrication of the channels of the
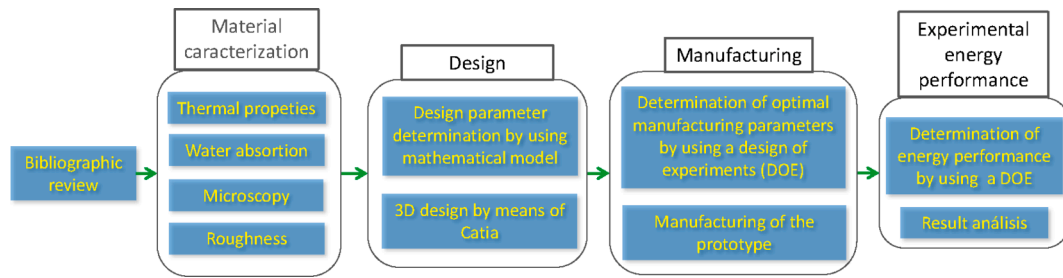
Fig. 1. Research methodology flowchart.
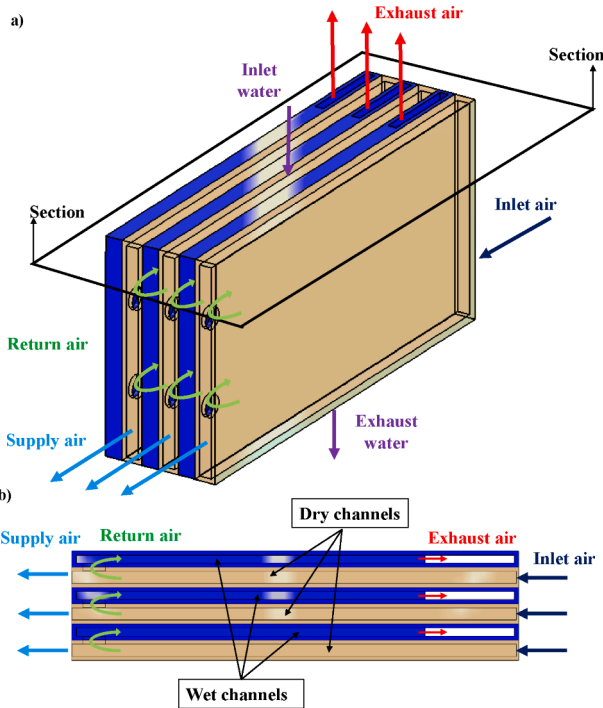
Fig. 2. A) 3d scheme of the diec channels. b) 2d section of the diec system.

DIEC system: (a) polylactic acid (PLA) with a 0.55% volume ratio of bronze (which provides a golden colour) is used as hydrophobic material with improved thermal conductivity; and (b) polyvinyl alcohol (PVA) with felt (fibrous format), which give rise to a resulting porous material with hydrophilic properties when polymer matrix (PVA) is finally removed. PVA is a water-soluble material, so it was used as a support to print felt. Therefore, when the material of PVA with felt was immersed in water, the PVA dissolved and the felt fibres remain as a microporous object. FFF technology was used as a manufacturing method, which is a great innovation since no bibliography was found on the matter. Both materials were supplied in the wire format with a diameter of 1.75 mm to allow their suitable processing by the FFF technology. Figure S1 presents a schematic of FFF manufacturing process. This AM method requires the realisation of a CAD design of the part to be manufactured as a first step. Subsequently, the 3D design is processed by specific software and cut into several layers. Finally, the 3D object is obtained by extruding a suitable thermoplastic material layer by layer on the print bed of a 3D printer.

The two materials were characterised in terms of water absorption capacity, according to ISO 62 [48], thermal conductivity, according to ISO 22007–4 [49], and Heat Deflection Temperature (HDT) (Table 2). Regarding water absorption, Method 1 of ISO 62 standard was applied to both materials. According to this method, samples were dried for 24 h at 50 °C prior to be immersed into distilled water at 23 °C. The samples

Table 2

Equipment parameters.

Function	Instrument	Model and manufacturer
Measured of HDT	Deflex/Vicat	HDT-VICAT MP3, ATS-FAAR, Italy
Measured of ρ	Helium pycnometer	G-DenPyc 2900, Gold APP Instruments, China
Measured of c_p	DSC	DSC Q20, TA Instruments, EEUU
Measured of α	Laser flash thermal constant analyser	LFA 1000, Linseis, Germany
Measured of microstructure	SEM	JSM-7800F, Jeol, Japan
Cool samples	Cryostat	CM1950, Leica, Spain
Cut samples	Microtone	RM2255, Leica, Spain
Roughness	Confocal and interferometric microscope	DCM8, Leica, Llobregat, Spain

were weighed every certain period of time to determine the water absorption. The ISO 62 standard established the weighing of the samples at 24 h, 48 h, 96 h, 192 h, etc. However, in this case, due to the fact that the water saturation of the material happened relatively quickly, the period time for the weighing was set to 1 min, 5 min, 10 min, 30 min, 60 min, 120 min, 180 min, 240 min, and 300 min. The samples manufactured for the water absorption tests are shown in Fig. 3. The parameters obtained from these tests were: (a) the water absorbed with respect to the weight of the dry samples throughout the entire test (W); (b) the percentage of water absorbed at saturation point (state of the material when it is not capable of absorbing more moisture under the established conditions) with respect to the weight of the dry samples (WSP); and (c) the percentage of water absorbed during the first 10 min with respect to the maximum water absorption (W10M).

Regarding thermal properties of both materials, density (ρ) was
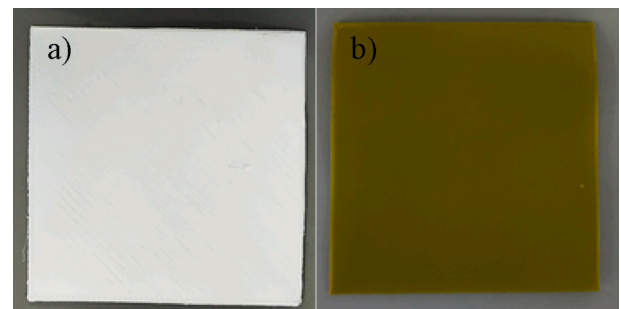
Fig. 3. Samples for water absorption test: a) porous material (Felt) and b) hydrophobic material (PLA with bronze).

measured by means of Helium pycnometer, specific heat capacity (c_p) by means of differential scanning calorimetry and diffusivity (α) by means of laser flash thermal constant analyser (Table 2). Samples with a radius of 25 mm and thickness of 5 mm were manufactured in order to perform all of these tests (Fig. 4). For diffusivity measurements, an additional layer of graphite was applied to the top and bottom of the samples to absorb the light from the laser flash. The results of the previous tests and using Eq. (1) allowed to determine the thermal conductivity (σ) of the materials.

$$\sigma = \rho \cdot c_p \cdot \alpha \tag{1}$$

The microstructure of the materials, both in filament form and in their final arrangement after being processed by FFF were examined by scanning electron spectroscopy (SEM) (Table 2). The samples were covered with paraffin, subsequently cooled in a cryostat (Table 2) at 0 °C and finally appropriately cut using a microtome (Table 2) to obtain an adequate cross section for their SEM analysis.

Additionally, the roughness and surface of a sample made of PLA with bronze and another of felt were measured by means of a confocal and interferometric microscope (Table 2). For these tests, the same samples manufacture for the conductivity test (Fig. 4) were used. The following parameters were measured: (a) arithmetic mean roughness, the average difference between peaks and valleys in a reference line, Ra; (b) maximum distance between peaks and valleys in a reference line, Rt; (c) average of the maximum peak-valley distances in a reference line; Rz; (d) mean squared of the deviation of the roughness profile from a reference line, Rq; (e) maximum peak height over the entire surface, Sp; (f) maximum valley depth in the entire surface, Sy; (g) maximum peak-valley distance in the entire surface, Sz; (h) mean squared of the height in the entire surface, Sq; (i) arithmetic mean height of the entire surface, Sa.

2.3. Design and manufacturing optimisation of the DIEC system

The design of DIEC system was carried out from a detailed mathematical model of dew-point indirect evaporative cooler developed in a previous research work [47]. The DIEC model was based on effectiveness (ε) and the Number of Transfer Units (NTU) method, which took into account the wet surface fraction of the return air channels of the HE. The model allowed obtaining the optimal design of the DIEC system and analysing its energy behaviour prior to manufacturing. The input data were DIEC system design parameters (Table 3) as well as inlet temperature, inlet humidity, volumetric air flow rate and ratio of volumetric air flow rate (R). The final result of applying the mathematical model were mainly the values of energy efficiency ratio (EER) and dew-point effectiveness (e_d). Different DIEC system design configurations were analysed to maximise EER and e_d. After defining the design parameters (Table 3), the CAD was carried out. Table 4.

The CAD of the heat and mass exchanger of the DIEC system is shown in Fig. 5a, as well as details of the water inlet holes, see Fig. 5b, and the wall perforations for return air and exhaust air, Fig. 5c. The DIEC system can be divided into two parts, the outer and the inner part. The outer one
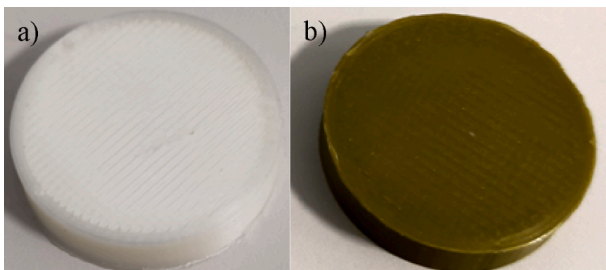
Fig. 4. Samples for conductivity tests. a) Porous material (Felt); and b) hydrophobic material (PVA with bronze).

Table 3
Design parameters of DIEC system.

Design parameter	Units	Value
Length	m	0.4
Width	m	0.484
Height	m	0.138
Number of channels	–	80
Inner wall thickness	mm	0.8
Outer wall thickness	mm	5
Channel height	mm	15.3
Channel width	mm	3
Returned /inlet airflow ratio (R)	–	0.5

Table 4
Values of the manufacturing parameters for the DOE.

N	Z (mm)	V (mm/s)	T (°C)	F (%)	t (min)
1	0.15	35	190	80	189
2	0.15	45	200	85	169
3	0.15	55	210	90	156
4	0.2	35	200	90	137
5	0.2	45	210	80	123
6	0.2	55	190	85	115
7	0.25	35	210	85	106
8	0.25	45	190	90	96
9	0.25	55	200	80	92
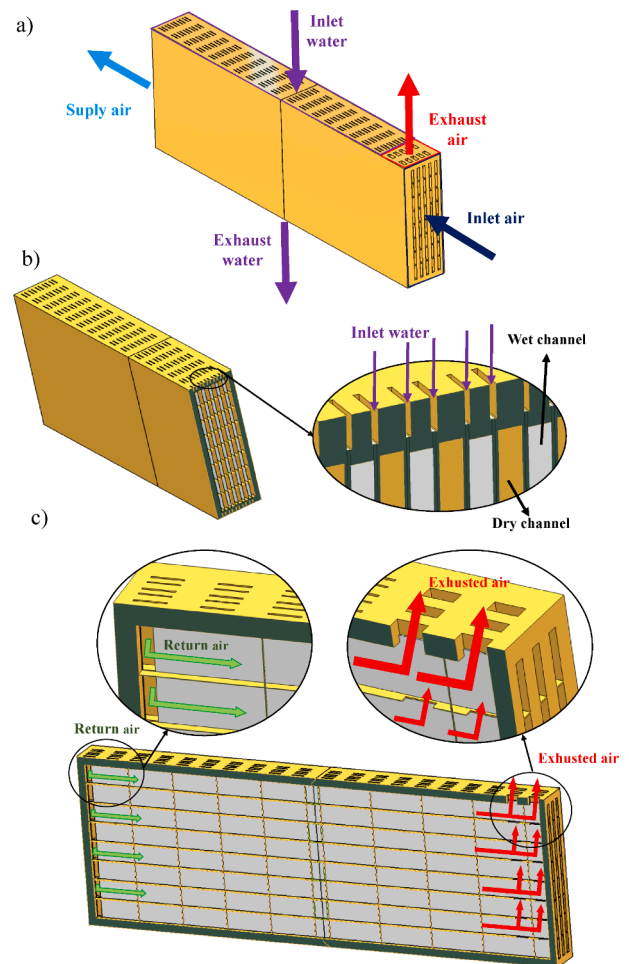
Fig. 5. Dew-point indirect evaporative cooling system CAD. a) Full DIEC system, b) DIEC cross section, c) DIEC section along a wet channel.

is the external shell which was designed primarily as a suitable support for the inner part, which is all the interior walls or plates. The internal part of the DIEC system was designed with an optimal wall thickness to increase heat transfer between channels. A thickness of 0.4 mm was chosen for each material, thus walls were manufactured with a total thickness of 0.8 mm, being 0.5 mm the minimum wall thickness allowed for conventional FFF systems [31]. The outer part was designed with a greater thickness, 5 mm, in order to improve the mechanical resistance of the prototype.

The statistical technique of design of experiments (DOE) was used in order to achieve the optimal manufacturing parameters using FFF technology. The DOE performance was based on the Taguchi L9 methodology [50]. Four input parameters were considered:

- Layer height (Z). This parameter is closely related to the diameter of the extruder and it is not recommended to reach a layer height greater than 75% of the diameter of the extruder [51].
- Extrusion speed (V). Above 65 mm/s there are clogging problems in the extruder according to the Tenlog TL-D3 Pro printer manufacturer, Tenlog.
- Temperature (T). The range studied was based on the parameters recommended by the suppliers of the material in thread format (190–210 °C).
- Flow (F). This parameter manages the amount of extruded material, increasing or decreasing it if necessary, thereby reducing material extrusion and preventing overlapping issues [52].

The DOE Taguchi L9 required 9 different tests with three levels for each of the four parameters, see Table 4. Sample quality and printing time were analysed for each test. A specific part of the DIEC system was manufactured to carry out the DOE. This part presented the minimum volume necessary to adequately replicate the complexity of the entire DIEC system and allowed to achieve representative results in a reasonable manufacturing time.

Four output parameters were taken into account in order to thoroughly analyse the DOE results: (a) degree of String formation in the Porous material (SP), (b) layer Joining and surface Quality in Porous material (JQP), (c) degree of String formation in the hydrophobic material (SH), and (d) layer Joining and surface Quality in Hydrophobic material (JQH). String formation (otherwise known as oozing, stringing or drooling) appear when small strings of plastic remain in a 3D printed model. Finally, according to the DOE results, the more suitable parameters were selected to manufacture the entire DIEC system.

2.4. Overall experimental energy performance of the DIEC system

An experimental setup was used to analyse the energy behaviour of the manufactured DIEC system. A schematic of this experimental setup is represented in Fig. 6. The experimental plant allowed adjusting the input air conditions, temperature, humidity and air flow rate, with an air handing unit (AHU). A detailed description of the experimental plant and the technical characteristics of the HVAC elements was included in a previous study [53].

The experimental setup was also composed of a set of sensors of dry bulb temperature (T), dew point temperature (T_d) and pressure difference (ΔP). The location of these sensors is shown in Fig. 6. The type of sensor and its accuracy are shown in Table 5. The sampling time was 3 s and the values were averaged every 15 min.

An additional DOE was also performed to analyse the energy behaviour of the DIEC system, applying a two level Factorial design. The input variables were inlet dry bulb temperature, T_i, dew-point air temperature, $T_{d,i}$, volumetric air flow rate, $\dot{V}_i$, and ratio of volumetric air flow rate, R, and the output variables were the differences in air temperature and air pressure between the inlet flow and the supply flow, ΔT and ΔP, respectively. The study consisted of 18 experimental tests, including two central points, as shown in Table 6. T_i ranged from 30 °C to 45 °C, $T_{d,i}$ ranged from 7.5 °C to 22.5 °C, $\dot{V}_i$ ranged from 90.5 m³/h to 120 m³/h and R ranged from 0.4 to 0.6.

The energy performance of the DIEC system was evaluated according to the following parameters:

- Sensible thermal energy delivered by the DIEC system to the supply air ($\dot{Q}_{cooling}$). Where $\dot{V}_{SA}$ is the supply volumetric air flow rate, ρ is the

Table 5
Technical specifications of the sensors.

Variable	Type of sensor	Manufacturer	Accuracy
T	PT100	GE Measurement and Control Solutions	± 0.2 °C
T_d	Chilled mirror hygrometer	GE Measurement & Control Solutions	± 0.15 °C
ΔP	Differential pressure transmitter	Siemens	± 5 % (at range < 500 Pa)
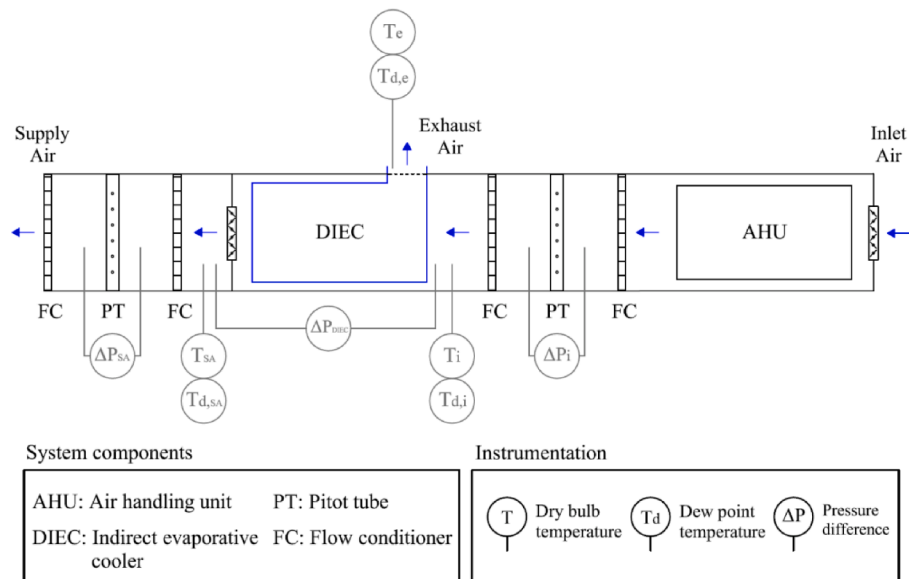
Fig. 6. Schematic of the DIEC experimental setup.

Table 6
Experimental tests of the manufactured DIEC system.

N	T_i [°C]	$T_{d,i}$ [°C]	$\dot{V}_i$ [m³/h]	R [-]	N	T_i [°C]	$T_{d,i}$ [°C]	$\dot{V}_i$ [m³/h]	R [-]
1	30	7.5	90.5	0.4	10	45	22.5	90.5	0.4
2	30	7.5	90.5	0.6	11	30	22.5	120	0.4
3	45	7.5	120	0.4	12	30	22.5	90.5	0.4
4	45	7.5	90.5	0.4	13	30	22.5	120	0.6
5	45	7.5	90.5	0.6	14	45	22.5	120	0.6
6	30	7.5	120	0.4	15	30	22.5	90.5	0.6
7	30	7.5	120	0.6	16	45	22.5	90.5	0.6
8	45	7.5	120	0.6	17	37.5	15	105.25	0.5
9	45	22.5	120	0.4	18	37.5	15	105.25	0.5

air density, and Δh is the difference in air enthalpy between the inlet flow and the supply flow.

$$\dot{Q}_{cooling} = \dot{V}_{SA} \cdot \rho \cdot \Delta h \tag{2}$$

- Electric energy consumption of the DIEC system ($\dot{W}$) considering a fan efficiency (η_{Fan}) of 0.5.

$$\dot{W} = \frac{\Delta P \cdot \dot{V}_i}{\eta_{Fan}} \tag{3}$$

- Energy Efficiency Ratio (EER) of the DIEC system, which measures the ratio between $\dot{Q}_{cooling}$ and $\dot{W}$.

$$EER = \frac{\dot{Q}_{cooling}}{\dot{W}} \tag{4}$$

- Dew-point effectiveness (e_d) of the DIEC system, defined as the ratio between the difference of inlet (T_i) and supply (T_{SA}) air dry-bulb temperatures, and the difference of T_i and inlet dew-point ($T_{d,i}$) temperatures.

$$e_d = \frac{T_i - T_{SA}}{T_i - T_{d,i}} \tag{5}$$

3. Results and discussions

This section shows an analysis of the materials used to manufacture the DIEC system, an evaluation of the manufacturing process and an experimental study of its energy performance.

3.1. Material analysis

The designed DIEC system was manufactured using two different filaments, PVA with felt and PLA with bronze. These materials in filaments format were experimentally analysed in this section. Images of both types of filaments, made with a scanning electron microscope (SEM), are shown in Fig. 7. It can be observed that the filament of PVA with felt presented a homogeneous surface before removing the PVA material, without the presence of fibres or pores (Fig. 7a and 7b). Therefore, this surface does not favour the inlet water that circulates through the wet channels to be retained by the material. However, clear differences in the surface of the material were obtained between the material with PVA and felt (Fig. 7b) and this material without PVA (Fig. 7c). The image in Fig. 7c, felt without PVA, shows a rough surface, with a pore size of the order of 6 μm, where the fibres were clearly aligned with the direction of extrusion. A side view of the junction of the two filaments, felt without PVA (left filament) and PLA with bronze (right filament), is shown in Fig. 7d. This figure also shows that the layer
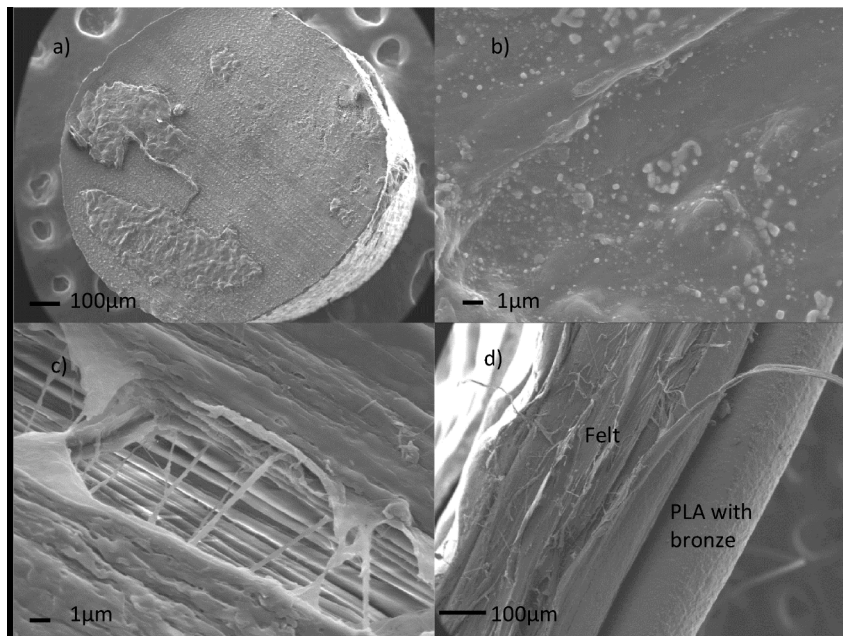
Fig. 7. SEM images: a) cross section of the filament of PVA with felt, b) Surface of a sample manufactured by FFF using the filament of PVA with felt, c) Surface of a sample manufactured by FFF using the filament of PVA with felt, when PVA is removed, d) Side view of a part manufactured by FFF technology using the filament of PVA with felt, when PVA is removed (left) and the filament of PLA with bonze (right).

of PLA with bronze material presented a continuous, smooth and pore-free surface, typical of materials with hydrophobic behaviour.

3.2. Analysis of the thermal and absorption properties

Several properties of the two filaments used to manufacture the DIEC system were obtained experimentally: c_p, α, ρ, σ, HDT, WSP and W10M, which were described in section 2.2. Moreover, the results of these properties were compared with those of a standard PLA filament (PLA-3D850) for 3D printing [54]. The results of the properties are shown in Table 7. It can be observed that thermal conductivity (σ) of PLA with bronze was 0.056 W/m·K higher that PLA-3D850. The HDT results showed that the maximum working temperature of PLA with bronze was 60 °C. The HDT value of the sample of felt without PVA was not obtained, since it is a flexible material, so correct values would not be obtained. Nevertheless, it was found in the literature that the maximum working temperature of the felt fibre was much higher than that polymers [55]. Therefore, the maximum working temperature of the DIEC system was determined by the PLA with bronze.

The water absorption capacity (W) was also obtained for both materials. W is one of the most critical parameters on cooling capacity of DIEC systems [40]. For this study, 3 samples of each filament were carried out. The results of W over 180 min for the felt samples were represented in Fig. 8. The W values for the PLA with bronze and PLA-3D850 samples were very low (around 0%) compared to felt ones, so they were not plotted. These curves of the felt material showed a clear logarithmic trend, see Fig. 8. Approximately 10 min after immersion, the samples had already absorbed 40% of the total amount of water that it could absorb, and 120 min later, the saturation point was reached. It was also observed that when saturation point was reached, about 32 wt% of the sample was composed of water. Comparing these results with those of another porous material such as kraft paper, it was concluded that they presented very similar values. Kraft paper reaches saturation point 120 min after the start of immersion, and 50% of the total water absorption occurs in the first 10 min [56].

3.3. Manufacturing results

Prior to the manufacture of the DIEC system, a DOE for the manufacture of the DIEC system was performed, in order to improve print quality. The parameters varied in the DOE were: Z, V, F and T, see Table 4. The DOE results are shown in Table 8. The results were qualitatively analysed visually and showed that a low temperature, 190 °C (tests 1, 6 and 8), generated a weak bond between the layers in both materials, especially when the flow (F) was also low, 80% (test 1). The low printing temperature reduced the amount of extrusion of material, due to the lower flow rate of the material, decreasing the bond between layers. For the highest temperatures, 210 °C (tests 3, 5 and 7), excessive stringing was observed in both materials, especially when the speed was not set to the minimum value (tests 3 and 5). Therefore, the best results (in general suitable SP, JQP, SH and JQH) were obtained using an appropriate combination of parameters (tests 2, 4 and 9). Specifically, among all these tests, test 9 presented the best results due to the fact that a higher layer height and manufacturing speed.

A final prototype was manufactured using the optimal parameters

Fig. 8. Results of water absorption tests.

obtained from the DOE: Z (0.25 mm), V (55 mm/s), T (190 °C) and F (80–85%), see Fig. 9. Under these processing conditions, the manufacturing time was significantly reduced and the quality of the final prototype was maximised.

The flow of the hydrophobic material was adjusted to 80% and the flow of the porous material to 85% in order to prevent the accumulation of the latter when the extruder changes direction during the manufacturing process (Fig. 9). The printed temperature was set to 190 °C for both materials, which resulted in slightly less string formation for both materials (Fig. 9). However, at higher temperatures, 200 °C for the hydrophobic material and 210 °C for the porous material, a significant number of strings were generated (Table 8).

Fig. 10 shows the positioning of the print bed, also known as print orientation. This print orientation selected improved the quality of the final prototype, since it allowed the adjoining material layers to adhere more suitably to each other, creating a stronger bond between the layers and therefore a mechanically stronger prototype. However, it also involves some drawbacks, as the inner walls needed some support below them in order to achieve an optimal result (Fig. 10). The maximum distance between supports was set at 15 mm, after some tests modifying this parameter. The distance between supports is actually the length of the bridge, which represents the length of the material that was printed without any support below it.

Images of the DIEC system manufactured and some interior sections are showed in Fig. 11. It can be seen that the manufactured system was similar to the DIEC design developed (bottom right image), Fig. 11a. The upper black part allowed the constant entry of water into the system. Fig. 11b shows a longitudinal section with a dry channel, a wet channel and perforations at the end of the channels, which allow the return air to recirculate from the dry channel to the wet channel. Finally, Fig. 11c shown several dry and wet channels, together with the supports that made FFF manufacturing possible.

3.4. Experimental performance

Experimental tests were carried out to analyse the energy behaviour of the manufactured DIEC system, see Table 6. First, the main cross effects of the input variables on ΔT and ΔP were studied, as shown in Fig. 12. For this analysis, the average value of each input variable was used as reference condition ($T_i = 37.5$ °C; $T_{d,i} = 15$ °C; $\dot{V}_i = 105.25$ m³/h; $R = 0.5$). It can be observed that ΔT increased when T_i and R were raised and $T_{d,i}$ and $\dot{V}_i$ were reduced. The most influential variables on ΔT, ordered from most to least influential, were T_i, R, $T_{d,i}$, $\dot{V}_i$. For this case study, the highest ΔT value was 19.8 °C for T_i equal to 45 °C and the average value of the remaining input variables. Regarding ΔP, an increase of $\dot{V}_i$ and R caused an increase in ΔP. T_i and $T_{d,i}$ had a very low influence on ΔP. For this case study, the highest ΔP value was 1095 Pa for R equal to 0.6 and the average value of the remaining input variables.

The results of $\dot{Q}_{cooling}$, $\dot{W}$, EER and ε_d for the set of experimental tests are shown in Table 9. These parameters were obtained from Eq. (2), 3, 4 and 5, respectively. The maximum $\dot{Q}_{cooling}$ value was 448.80 W, reached

Table 7
Thermal and absorption characterisation of materials.

Material	Cp [J/g·K]	α [m²/s]	ρ [kg/m³]	σ [W/m·K]	HDT [°C]	WSP [%]	W10M [%]
Felt	2.095	9.92	1138.6	0.239	——	32	40
PLA with bronze	1.945	816.0	1278.1	0.261	60	0.1	0
PLA-3D850	1.07	15.4	1240.0	0.205	55	0.1	0

Table 8
Results of DOE for the manufacture of the DIEC system.

Test number	Appearance	Degree of String formation in the Porous material (SP)	layer Joining and surface Quality in Porous material (JQP)	String formation in the Hydrophobic material (SH)	Layer Joining and surface Quality in Hydrophobic material (JQH)
1		Slight stringing	Low quality	Slight stringing	High quality
2		Suitable stringing	Suitable quality	Suitable stringing	High quality
3		Excessive stringing	Suitable quality	Excessive stringing	Low quality
4		Suitable stringing	Suitable quality	Suitable stringing	Suitable quality
5		Excessive stringing	Suitable quality	Excessive stringing	Suitable quality
6		Slight stringing	Suitable quality	Slight stringing	Suitable quality
7		Excessive stringing	Suitable quality	Excessive stringing	Suitable quality
8		Slight stringing	Suitable quality	Slight stringing	Low quality
9		Suitable stringing	Suitable quality	Suitable stringing	Suitable quality
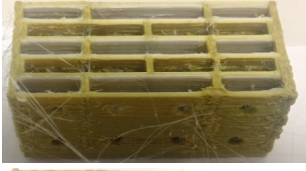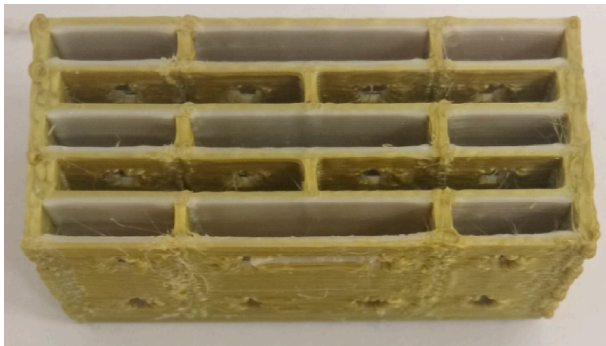
Fig. 9. Manufacturing result using with the optimal set of parameter.
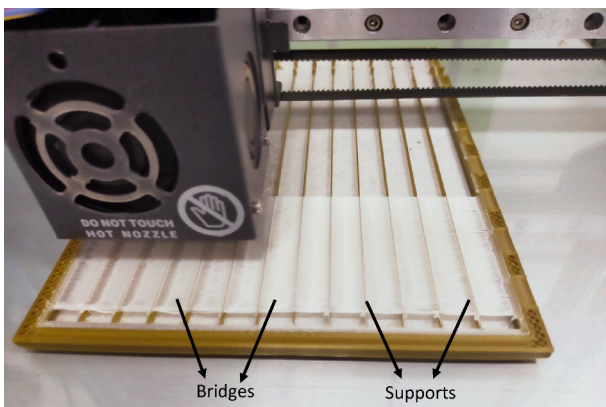
Fig. 10. Section of DIEC system during the manufacturing process.

for N3, i.e. $T_i = 45\ ^\circ C$, $T_{d,i} = 7.5\ ^\circ C$, $\dot{V}_i$=120 m³/h and R = 0.4. These inlet conditions correspond to warm and dry air conditions and the maximum supply air flow. For this case study, the values of $\dot{W}$, EER and ε_d were 34.59 W, 12.97 and 0.5, respectively. A high EER value was achieved for N10, 22.74. The inlet conditions of this test were $T_i = 45\ ^\circ C$, $T_{d,i} = 22.5\ ^\circ C$, $\dot{V}_i$=90.5 m³/h and R = 0.4. This result was mainly due to the low electrical consumption of the fan for low $\dot{V}_i$ values. Regarding ε_d, high values were also obtained, up to 0.90 for high values of T_i (45 °C), $T_{d,i}$ (22.5 °C) and R (0.6), N14. Therefore, the manufactured system showed great cooling capacity and high energy performance under different climatic conditions.

The relationships between the inlet air conditions (T_i and $T_{d,i}$) and $\dot{Q}_{cooling}$ and EER were also studied, see Fig. 13. The remaining input variables were fixed at constant values: $\dot{V}_i$=90.5 m³/h; R = 0.4. It can be observed that the $\dot{Q}_{cooling}$ values increased significantly when T_i increased from 30 °C to 45 °C, see Fig. 13a. $T_{d,i}$ had low influence on $\dot{Q}_{cooling}$ compared to T_i. These influences are in agreement with the ΔT values shown in Fig. 12. For this case study, the $\dot{Q}_{cooling}$ values ranged between 100 W and 350 W. The trend of EER was similar to that of $\dot{Q}_{cooling}$ when T_i increased from 30 °C to 45 °C, see Fig. 13b. Slight variation of $\dot{W}$ was obtained for different $T_{d,i}$ values, since $T_{d,i}$ had a low influence on ΔP, as shown in Fig. 12, so the EER variation was also slight. The maximum EER value was 22.74 for a high T_i value. These results showed that the system improved its energy performance under more unfavourable conditions, that is, high values of T_i and $T_{d,i}$.

Finally, a comparative analysis of the DIEC system manufactured by FFF with respect to other DIEC systems manufactured by traditional means was carried out (Table 10). For inlet conditions of $T_{d,i}$ (10.7–22.5) and T_i (27.5–35.5), the EER values found in the literature were between 8.3 and 34.2 which are higher than those of the DIEC system studied (7.83) with the same inner condition. However, for higher inlet
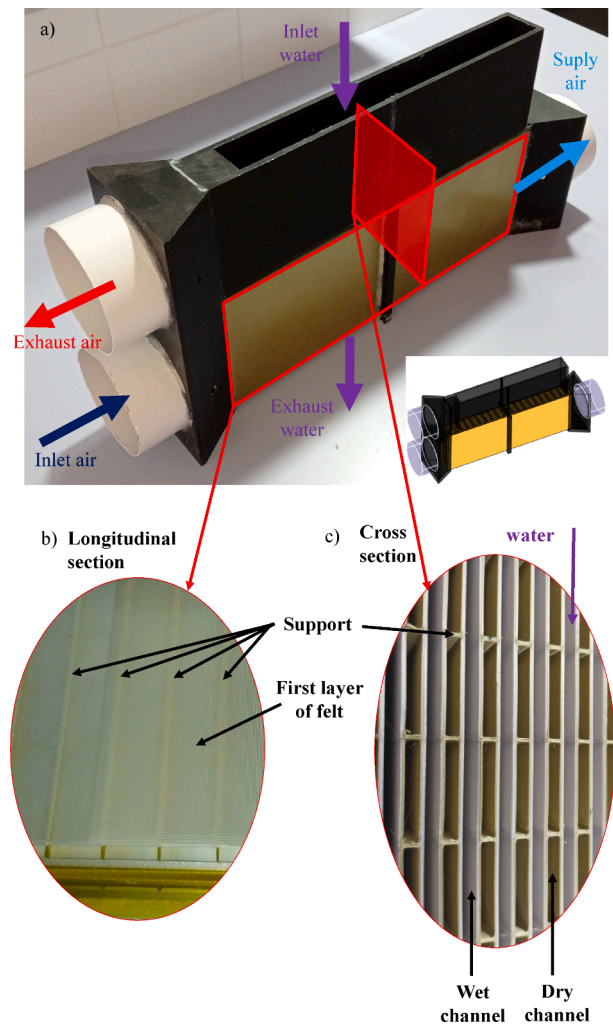
Fig. 11. A) manufactured diec system and its cad at the bottom right, b) diec system longitudinal section, c) diec system cross section.
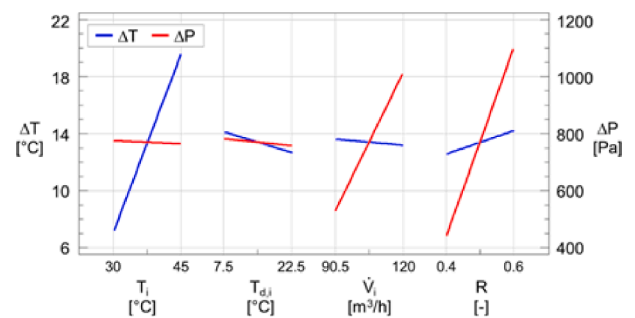
Fig. 12. Effect of inlet conditions on outputs of the DOE: ΔT and ΔP.

temperature, EER values of up to 22.74 were achieved. Regarding ε_d, in literature values between 0.41 and 0.91 were observed when similar inlet conditions were analysed, which is in agreement with the value obtained in the DIEC prototype studied, 0.78. Zhan *et al.* [57] achieved a slightly better ε_d (0.91) than that of the present work, however, the length of the channels used for Zhan *et al.* [57] was greater than 1 m, so the heat exchange volume was higher. Lee *et al.* [58] studied a DIEC system with a shorter channel length (0.35 m), and the dew point effectiveness value was reduced (up to 0.75–0.9), reaching similar values to those achieved in the present study. When it comes to the pressure drop, lower EER and similar or lower ε_d were identified in

Table 9

Experimental results of $\dot{Q}_{cooling}$, $\dot{W}$, EER and ε_d.

N	$\dot{Q}_{cooling}$ [W]	$\dot{W}$ [W]	EER [-]	ε_d [-]	N	$\dot{Q}_{cooling}$ [W]	$\dot{W}$ [W]	EER [-]	ε_d [-]
1	144.98 ± 10.6	17.08 ± 1.0	8.49 ± 0.5	0.36 ± 0.010	10	319.28 ± 21.4	14.04 ± 0.8	22.74 ± 1.5	0.78 ± 0.009
2	100.76 ± 7.3	36.52 ± 0.3	2.76 ± 0.3	0.37 ± 0.010	11	133.44 ± 10.8	36.35 ± 2.3	3.67 ± 0.2	0.74 ± 0.029
3	448.80 ± 29.9	34.59 ± 2.1	12.97 ± 1.1	0.50 ± 0.006	12	120.00 ± 9.1	15.32 ± 0.9	7.83 ± 0.5	0.87 ± 0.030
4	343.90 ± 22.9	18.02 ± 1.1	19.08 ± 1.3	0.51 ± 0.006	13	101.44 ± 7.8	93.71 ± 3.9	1.08 ± 0.1	0.85 ± 0.030
5	263.05 ± 17.4	36.43 ± 1.5	7.22 ± 0.5	0.58 ± 0.005	14	329.60 ± 21.9	92.26 ± 3.8	3.57 ± 0.2	0.90 ± 0.009
6	181.20 ± 13.4	36.16 ± 2.2	5.01 ± 0.4	0.34 ± 0.010	15	76.99 ± 5.9	33.58 ± 1.4	2.29 ± 0.2	0.85 ± 0.029
7	132.00 ± 9.6	91.38 ± 3.8	1.44 ± 0.1	0.37 ± 0.010	16	249.78 ± 16.6	33.58 ± 1.4	7.44 ± 0.5	0.89 ± 0.009
8	334.64 ± 22.3	91.38 ± 3.8	3.66 ± 0.2	0.56 ± 0.006	17	249.97 ± 16.9	39.61 ± 2.1	6.31 ± 0.4	0.63 ± 0.009
9	401.28 ± 26.9	34.59 ± 2.1	11.60 ± 0.9	0.74 ± 0.009	18	251.72 ± 17.0	38.72 ± 2.0	6.50 ± 0.4	0.64 ± 0.009
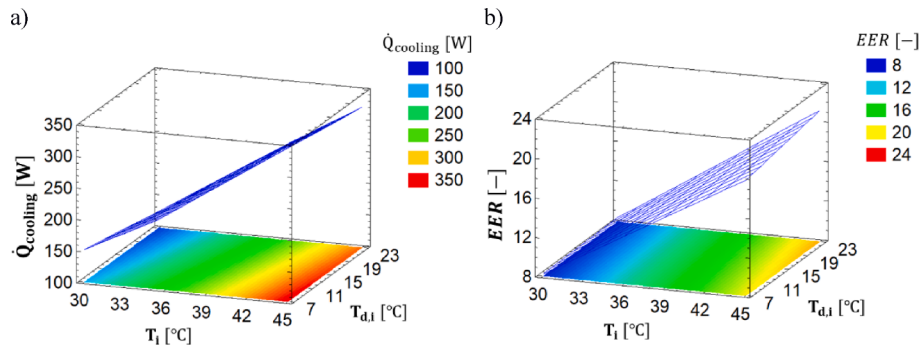
Fig. 13. Response surfaces and contour line plots of $\dot{Q}_{cooling}$ and EER on T_i and $T_{d,i}$.

Table 10

Analysis of performance parameters of DIEC developed by other authors.

Reference	Channel length [m]	Types of porous materials	$T_{d,i}$ [°C]	T_i [°C]	EER [-]	ε_d [-]
[56]	–	Cellulous fibre	10.7–11.4	29.6–35.7	8.30–11.80	0.41–0.48
[57]	1.00	Cotton	15.00	28.00	–	0.91
[58]	0.35	Porous layer coating	11.30–22.10	27.50–32.00	–	0.75–0.90
[59]	–	Polystyrene + Nylon	19.80	35.50	13.80	0.64
[59]	–	Coolmax fabric	22.10	28.80	34.20	0.81
[60]	–	Polystyrene + nylon fibre	21.00	35.50	13.80	0.71
Present study	0.40	Felt	7.50–22.50	30.00–45.00	1.44–22.74	0.36–0.90

literature for equivalent inlet conditions. That means the pressure drop in the channels of the prototype studied could be even a little bit higher than those found in literature, so for future work special attention should be paid to this matter.

4. Conclusions

In the present work, a dew-point indirect evaporative cooling (DIEC) system was designed, manufactured and experimentally evaluated. Hence, two materials suitable for use in Fused Filament Fabrication (FFF) techniques were analysed. One of the materials was composed of PLA with bronze (hydrophobic material) for the dry channels and another of PVA with felt (porous material) for the wet channels, analysing in both cases their thermal, absorption and roughness properties. PVA is a water-soluble material, with the main function of making it possible to manufacture parts with Felt material by means of FFF. The optimal design and operating parameters of the DIEC system to achieve the maximum cooling capacity were determined. Two Designs of Experiments (DOE) were performed for the fabrication and energy performance study of the DIEC system.

The results of the material analysis showed adequate values of thermal conductivity for use in the walls of the DIEC system, up to 27% higher than those of standard PLA. The Heat Deflection Temperature (HDT) value was also 9% higher when the PLA-based filament contained

bronze. These results favour the heat transfer and the reduction of the thermal resistance of the DIEC system. Water absorption tests showed that the felt material reached a high water absorption capacity in short periods of time. As a result, the evaporative effect and the cooling capacity of the prototype are improved. Surface tests showed that the felt material also had high roughness, which is in alignment with its higher water absorption capacity. However, the roughness of the PLA with bronze material was up to 89% lower than that of the felt, so this fact reduced the pressure drop of the dry channels and increasing the energy performance of the system.

The conditions to achieve the optimal balance between the quality of the system parts and the manufacturing time used in the manufacturing process were obtained using high layer height, high extrusion speed, low temperature and intermediate material flows among all those values considered in the performed DOE. The optimal manufacturing parameters were used to develop a DIEC system. The experimental results of the energy evaluation of the DIEC system showed high Energy Efficiency Ratio, EER, values, up to 22.74, mainly due to high cooling capacity values, 320 W, and low electrical energy consumption values, 14 W. High dew-point effectiveness values were also obtained, up to 0.9, mainly under warm inlet weather conditions, 45 °C.

Therefore, the results presented show that FFF technology allows successfully manufacturing DIEC systems using hydrophilic and hydrophobic materials for dry and wet channels, respectively, thus improving

their cooling capacity and energy efficiency.

Declaration of Competing Interest

The authors declare that they have no known competing financial interests or personal relationships that could have appeared to influence the work reported in this paper.

Data availability

Data will be made available on request.

Acknowledgements

Appendix A. Supplementary material

Supplementary data to this article can be found online at https://doi.org/10.1016/j.applthermaleng.2023.120683.

References

[1] J. Castillo-González, F. Comino, F.J. Navas-Martos, M. Ruiz de Adana, Life cycle assessment of an experimental solar HVAC system and a conventional HVAC system, Energy Build. 256 (2022) 111697.

[2] F. Comino, J. Castillo González, F.J. Navas-Martos, M. Ruiz de Adana, Experimental energy performance assessment of a solar desiccant cooling system in Southern Europe climates, Appl. Therm. Eng. 165 (2020), 114579, https://doi.org/10.1016/j.applthermaleng.2019.114579.

[3] O. Amer, R. Boukhanouf, H.G. Ibrahim, A Review of Evaporative Cooling Technologies, Int. J. Environ. Sci. Dev. 6 (2) (2014) 111–117.

[4] Y. Wang, X. Huang, L.i. Li, Comparative study of the cross-flow heat and mass exchangers for indirect evaporative cooling using numerical methods, Energies. 11 (12) (2018) 3374.

[5] Z. Duan, X. Zhao, C. Zhan, X. Dong, H. Chen, Energy saving potential of a counter-flow regenerative evaporative cooler for various climates of China: Experiment-based evaluation, Energy Build. 148 (2017) 199–210, https://doi.org/10.1016/j.enbuild.2017.04.012.

[6] E. Rasouli, E. Fricke, V. Narayanan, High efficiency 3-D printed microchannel polymer heat exchangers for air conditioning applications, Sci. Technol. Built Environ. 28 (2022) 289–306, https://doi.org/10.1080/23744731.2022.2026693.

[7] J. Boxleitner, T. Mulholland, N. Gregory, Air-to-Liquid Heat Exchanger Fabricated Using Deposition-Based Additive Manufacturing Process, J. Therm. Sci. Eng. Appl. 14 (2021), https://doi.org/10.1115/1.4054447.

[8] I. Kaur, P. Singh, State-of-the-art in heat exchanger additive manufacturing, Int. J. Heat Mass Transf. 178 (2021), 121600, https://doi.org/10.1016/j.ijheatmasstransfer.2021.121600.

[9] S. Lowrey, C. Hughes, Z. Sun, Thermal-hydraulic performance investigation of an aluminium plate heat exchanger and a 3D-printed polymer plate heat exchanger, Appl. Therm. Eng. 194 (2021), 117060, https://doi.org/10.1016/j.applthermaleng.2021.117060.

[10] A. Sapienza, V. Brancato, Y. Aristov, S. Vasta, Plastic heat exchangers for adsorption cooling: Thermodynamic and dynamic performance, Appl. Therm. Eng. 188 (2021), 116622, https://doi.org/10.1016/j.applthermaleng.2021.116622.

[11] M.A. Arie, D.M. Hymas, F. Singer, A.H. Shooshtari, M. Ohadi, An additively manufactured novel polymer composite heat exchanger for dry cooling applications, Int. J. Heat Mass Transf. 147 (2020) 118889, https://doi.org/10.1016/j.ijheatmasstransfer.2019.118889.

[12] P. Singh, A. Odukomaiya, M.K. Smith, A. Aday, S. Cui, A. Mahvi, Processing of phase change material by fused deposition modeling: Toward efficient thermal energy storage designs, J. Energy Storage. 55 (2022), https://doi.org/10.1016/j.est.2022.105581.

[13] M. ToksoyKaradeniz, Z. Haktan, 3D printing of HVAC systems, REHVA J. (2017) 18–22.

[14] S.A. Niknam, M. Mortazavi, D. Li, Additively manufactured heat exchangers: a review on opportunities and challenges, Int. J. Adv. Manuf. Technol. 112 (2021) 601–618, https://doi.org/10.1007/s00170-020-06372-w.

[15] L. Fontana, P. Minetola, F. Calignano, L. Iuliano, M.S. Khandpur, V. Stiuso, Experimental testing of 3D printed polymeric heat exchangers, IOP Conf. Ser. Mater. Sci. Eng. 1136 (1) (2021) 012047.

[16] Z. Huang, J. Ling, Y. Hwang, V. Aute, R. Radermacher, Design and numerical parametric study of a compact air-cooled heat exchanger, Sci. Technol. Built Environ. 23 (2017) 970–982, https://doi.org/10.1080/23744731.2017.1335164.

[17] Swapneel Shailesh Danayat, Investigating 3-D Printed Polymer Heat Exchanger, Pap. Knowl. Towar. a Media Hist. Doc. 3 (2019) 49–58.

[18] R.A. Felber, G. Nellis, N. Rudolph, Design and modeling of 3D-printed air-cooled heat exchangers, Int. Refrig. Air Cond. Conf. (2016). http://docs.lib.purdue.edu/iracc/1763%0Ahttps://docs.lib.purdue.edu/iracc/1763/.

[19] U. Scheithauer, E. Schwarzer, T. Moritz, A. Michaelis, Additive Manufacturing of Ceramic Heat Exchanger: Opportunities and Limits of the Lithography-Based Ceramic Manufacturing (LCM), J. Mater. Eng. Perform. 27 (2017) 14–20, https://doi.org/10.1007/s11665-017-2843-z.

[20] S.M. Thompson, Z.S. Aspin, N. Shamsaei, A. Elwany, L. Bian, Additive manufacturing of heat exchangers: A case study on a multi-layered Ti-6Al-4V oscillating heat pipe, Addit. Manuf. 8 (2015) 163–174, https://doi.org/10.1016/j.addma.2015.09.003.

[21] D. Saltzman, M. Bichnevicius, S. Lynch, T.W. Simpson, E.W. Reutzel, C. Dickman, R. Martukanitz, Design and evaluation of an additively manufactured aircraft heat exchanger, Appl. Therm. Eng. 138 (2018) 254–263, https://doi.org/10.1016/j.applthermaleng.2018.04.032.

[22] L.i. Yi, M. Glatt, P. Sridhar, K. de Payrebrune, B.S. Linke, B. Ravani, J.C. Aurich, An eco-design for additive manufacturing framework based on energy performance assessment, Addit. Manuf. 33 (2020) 101120.

[23] A. Tarancón, V. Esposito, 3D Printing For Energy Applications, John Wiley Sons Inc, Hoboken, New Jersey, 2012. https://eur-lex.europa.eu/legal-content/PT/TXT/PDF/?uri=CELEX:32016R0679ampq;from=PT%0Ahttp://eur-lex.europa.eu/LexUriServ/LexUriServ.do?uri=CELEX:52012PC0011:pt:NOT.

[24] L. Pereira, The Effects of 3D Printing Parameters and Surface Treatments on Convective Heat Transfer Performance, Electron, Theses Diss, 2019. https://openprairie.sdstate.edu/etd/3155.

[25] R.P.P. da Silva, M.V.V. Mortean, K.V. de Paiva, L.E. Beckedorff, J.L.G. Oliveira, F.G. Brandão, A.S. Monteiro, C.S. Carvalho, H.R. Oliveira, D.G. Borges, V.L. Chastinet, Thermal and hydrodynamic analysis of a compact heat exchanger produced by additive manufacturing, Appl. Therm. Eng. 193 (2021) 116973.

[26] H. Prajapati, D. Ravoori, R.L. Woods, A. Jain, Measurement of anisotropic thermal conductivity and inter-layer thermal contact resistance in polymer fused deposition modeling (FDM), Addit. Manuf. 21 (2018) 84–90, https://doi.org/10.1016/j.addma.2018.02.019.

[27] M.A. Arie, A.H. Shooshtari, R. Tiwari, S.V. Dessiatoun, M.M. Ohadi, J.M. Pearce, Experimental characterization of heat transfer in an additively manufactured polymer heat exchanger, Appl. Therm. Eng. 113 (2017) 575–584, https://doi.org/10.1016/j.applthermaleng.2016.11.030.

[28] Y. Li, Z. Feng, L. Huang, K. Essa, E. Bilotti, H. Zhang, T. Peijs, L. Hao, Additive manufacturing high performance graphene-based composites: A review, Compos. Part A Appl. Sci. Manuf. 124 (2019), 105483, https://doi.org/10.1016/j.compositesa.2019.105483.

[29] D. Zhang, B. Chi, B. Li, Z. Gao, Y. Du, J. Guo, J. Wei, Fabrication of highly conductive graphene flexible circuits by 3D printing, Synth. Met. 217 (2016) 79–86, https://doi.org/10.1016/j.synthmet.2016.03.014.

[30] T. Mulholland, S. Goris, J. Boxleitner, T.A. Osswald, N. Rudolph, Fiber Orientation Effects in Fused Filament Fabrication of Air-Cooled Heat Exchangers, Addit. Manuf. Compos. Complex Mater. 70 (2018) 298–302, https://doi.org/10.1007/s11837-017-2733-8.

[31] A. Alafaghani, A. Qattawi, M.A. Ablat, Design Consideration for Additive Manufacturing: Fused Deposition Modelling, Open, J. Appl. Sci. 07 (2017) 291–318, https://doi.org/10.4236/ojapps.2017.76024.

[32] Y. Wan, J. Lin, K.J. Chua, C. Ren, Similarity analysis and comparative study on the performance of counter-flow dew point evaporative coolers with experimental validation, Energy Convers. Manag. 169 (2018) 97–110, https://doi.org/10.1016/j.enconman.2018.05.043.

[33] O. Khalid, Z. Butt, W. Tanveer, H.I. Rao, Design and experimental analysis of counter-flow heat and mass exchanger incorporating (M-cycle) for evaporative cooling, Heat Mass Transf. 53 (2016) 1391–1403, https://doi.org/10.1007/s00231-016-1914-2.

[34] O. Khalid, M. Ali, N.A. Sheikh, H.M. Ali, M. Shehryar, Experimental analysis of an improved Maisotsenko cycle design under low velocity conditions, Appl. Therm. Eng. 95 (2016) 288–295, https://doi.org/10.1016/j.applthermaleng.2015.11.030.

[35] Z. Duan, C. Zhan, X. Zhang, M. Mustafa, X. Zhao, B. Alimohammadisagvand, A. Hasan, Indirect evaporative cooling: Past, present and future potentials, Renew. Sustain. Energy Rev. 16 (2012) 6823–6850, https://doi.org/10.1016/j.rser.2012.07.007.

[36] C. T'Joen, Y. Park, Q. Wang, A. Sommers, X. Han, A. Jacobi, A review on polymer heat exchangers for HVAC&R applications, Int. J. Refrig. 32 (2009) 763–779, https://doi.org/10.1016/j.ijrefrig.2008.11.008.

[37] B. Porumb, P. Ungureşan, L.F. Tutunaru, A. Şerban, M. BĂlan,, A Review of Indirect Evaporative Cooling Technology, Energy Procedia. 85 (2016) 461–471, https://doi.org/10.1016/j.egypro.2015.12.228.

[38] B. Riangvilaikul, S. Kumar, An experimental study of a novel dew point evaporative cooling system, Energy Build. 42 (2010) 637–644, https://doi.org/10.1016/j.enbuild.2009.10.034.

[39] J. Woods, E. Kozubal, A desiccant-enhanced evaporative air conditioner: Numerical model and experiments, Energy Convers. Manag. 65 (2013) 208–220, https://doi.org/10.1016/j.enconman.2012.08.007.

[40] Z. Duan, X. Zhao, J. Li, Design, fabrication and performance evaluation of a compact regenerative evaporative cooler: Towards low energy cooling for buildings, Energy. 140 (2017) 506–519, https://doi.org/10.1016/j.energy.2017.08.110.

[41] C. Murphy, M. Collins, Microcrystalline Cellulose Reinforced Polylactic Acid Biocomposite Filaments for 3D Printing, Polym. Compos. 16 (2016) 101–113, https://doi.org/10.1002/pc.

[42] J. Rodríguez, D. Restrepo, Elaboración y caracterización de componentes plásticos porosos, mediante impresión 3d para aplicaciones de regeneración ósea, Univ. St. Tomás Div. Ing. Fac. Ing. Mecánica Bogotá D.C. 2015 (2015), https://doi.org/10.1145/3132847.3132886.

[43] J. Feng, J. Fu, C. Shang, Z. Lin, X. Niu, B. Li, Efficient generation strategy for hierarchical porous scaffolds with freeform external geometries, Addit. Manuf. 31 (2020), 100943, https://doi.org/10.1016/j.addma.2019.100943.

[44] B.M. Babel, C.J. Massar, J. Day, Material Processing of a HIPS / AC FDM Filament for Water Filtration Material Processing of a HIPS / AC FDM Filament for Water Filtration, (2018).

[45] W. Johnston, B. Sharma, Additive manufacturing of fibrous sound absorbers, Addit. Manuf. 41 (2021) 101984, https://doi.org/10.1016/j.addma.2021.101984.

[46] U. Kalsoom, C.K. Hasan, L. Tedone, C. Desire, F. Li, M.C. Breadmore, P. N. Nesterenko, B. Paull, Low-Cost Passive Sampling Device with Integrated Porous Membrane Produced Using Multimaterial 3D Printing, Anal. Chem. 90 (2018) 12081–12089, https://doi.org/10.1021/acs.analchem.8b02893.

[47] F. Comino, M.J. Romero-Lara, M. Ruiz de Adana, Experimental and numerical study of dew-point indirect evaporative coolers to optimize performance and design, Int. J. Refrig. 142 (2022) 92–102, https://doi.org/10.1016/j.ijrefrig.2022.06.006.

[48] Water absorption determination. Plastic, UNE-EN ISO 62. (2008) 22. Doi: M 49466:2008.

[49] INTERNATIONAL STANDARD conductivity and thermal diffusivity. Plastic, Int. Stand. ISO 22007-12017(E). 2017 (2017) 23. Doi: ISO 22007-4:2017(E).

[50] A. Alafaghani, A. Qattawi, Investigating the effect of fused deposition modeling processing parameters using Taguchi design of experiment method, J. Manuf. Process. 36 (2018) 164–174, https://doi.org/10.1016/j.jmapro.2018.09.025.

[51] P. Czyżewski, D. Marciniak, B. Nowinka, M. Borowiak, M. Bieliński, Influence of Extruder's Nozzle Diameter on the Improvement of Functional Properties of 3D-Printed PLA Products, Polymers (Basel). 14 (2) (2022) 356.

[52] P. Ferretti, C. Leon-Cardenas, G.M. Santi, M. Sali, E. Ciotti, L. Frizziero, G. Donnici, A. Liverani, Relationship between fdm 3d printing parameters study: Parameter optimization for lower defects, Polymers (Basel). 13 (13) (2021) 2190.

[53] F. Comino, F. Táboas, F. Peci, M. Ruiz de Adana, Detailed experimental analysis of the energy performance of a desiccant wheel activated at low temperature, Appl. Therm. Eng. 178 (2020), 115580, https://doi.org/10.1016/j.applthermaleng.2020.115580.

[54] E. Ivanov, R. Kotsilkova, H. Xia, Y. Chen, R. Donato, K. Donato, A. Godoy, R. Di Maio, C. Silvestre, S. Cimmino, V. Angelov, PLA/Graphene/MWCNT composites with improved electrical and thermal properties suitable for FDM 3D printing applications, Appl. Sci. 9 (6) (2019) 1209.

[55] Advanced Materials Engineering, (n.d.). https://www.final-materials.com/gb/308-high-temperature-felts-and-blankets.

[56] Z. Duan, Investigation of a novel dew point indirect evaporative air conditioning system for buildings, Univ, Nottingham, 2011. PhD Thesis,.

[57] C. Zhan, Z. Duan, X. Zhao, S. Smith, H. Jin, S. Riffat, Comparative study of the performance of the M-cycle counter-flow and cross-flow heat exchangers for indirect evaporative cooling - Paving the path toward sustainable cooling of buildings, Energy. 36 (2011) 6790–6805, https://doi.org/10.1016/j.energy.2011.10.019.

[58] J. Lee, D.Y. Lee, Experimental study of a counter flow regenerative evaporative cooler with finned channels, Int. J. Heat Mass Transf. 65 (2013) 173–179, https://doi.org/10.1016/j.ijheatmasstransfer.2013.05.069.

[59] J. Lv, H. Xu, M. Zhu, Y. Dai, H. Liu, Z. Li, The performance and model of porous materials in the indirect evaporative cooling system: A review, J. Build. Eng. 41 (2021), 102741, https://doi.org/10.1016/j.jobe.2021.102741.

[60] J. Li, L. Wang, L. Dai, L. Zhong, B. Liu, J. Ren, Y. Xu, Synthesis and characterization of reinforced acrylate photosensitive resin by 2-hydroxyethyl methacrylate-functionalized graphene nanosheets for 3D printing, J. Mater. Sci. 53 (2018) 1874–1886, https://doi.org/10.1007/s10853-017-1432-8.